Spectral Projections in NIMROD

Carl Sovinec

University of Wisconsin-Madison

Center for Extended MHD Meeting

November 10, 2013 Denver, Colorado

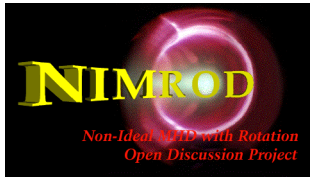

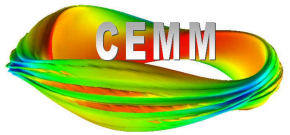

Thesis

Convergence from the stable side is achieved with a C^0 spectral-element representation by projecting flow-divergence and parallel vorticity at the limit of resolution.

Outline

- Introduction
- Spectral projection
  - bases for projection
  - auxiliary equations
- Results with NIMROD
- Brief asides on DKE and vacuum field
- Conclusions

Introduction: NIMROD's C^0 spectral-element implementation is formulated to allow dissipation for each physical field.

- Like conventional thermal-conduction and structural-mechanics applications, second-order derivatives lead to mathematical 'energy' increasing as the scale of oscillations decreases.
  - In 1D, for example:

$$-\frac{d^2v}{dx^2} = f \quad \Rightarrow \quad \int \frac{dw}{dx}\frac{dv}{dx}dx = \int wf\,dx \quad \text{for all } w \text{ in } H_e^1$$

  - Continuous functions are necessary, and they are sufficient in the sense that greater continuity is not required.
- First-order spatial derivatives do not provide a coercive energy. The following single-field formulation does not bound fine-scale oscillations.

$$-\frac{dv}{dx} = \frac{dv}{dt} \quad \Rightarrow \quad -\int w\frac{dv}{dx}dx = \int w\frac{dv}{dt}dx \quad \text{for all } w \text{ in } H_e^1$$

- *The extended-MHD dilemma is that physical dissipation is important but small, and interchange provides sources of energy at small scales.*

NIMROD's standard spectral-element representation with equal-order **V**, **B**, and *p* expansions converges on interchange from the unstable side.

- Test case is m=4, k=-1.78 Suydam mode at r_s=0.371 and $D_s(r_s)$=0.443.

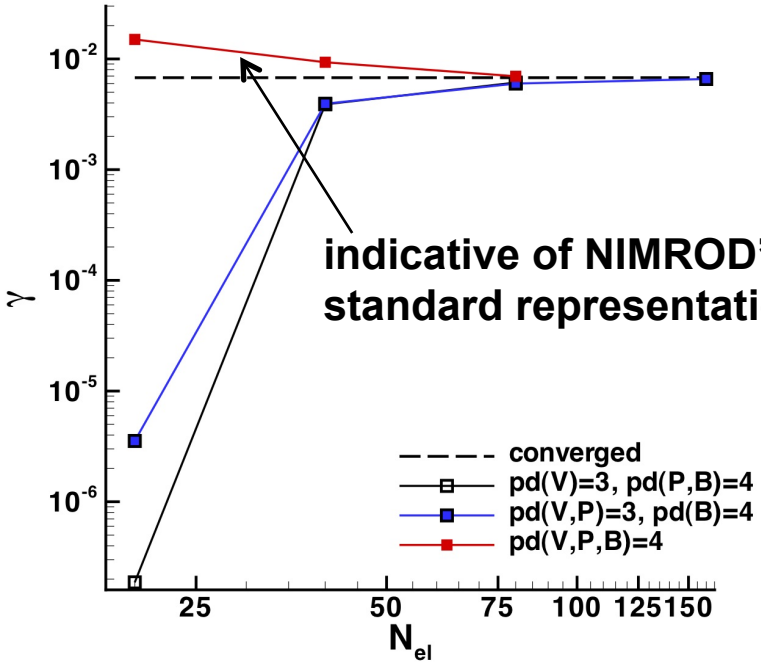

CYL_SPEC 1D eigenvalue results compare different expansions.

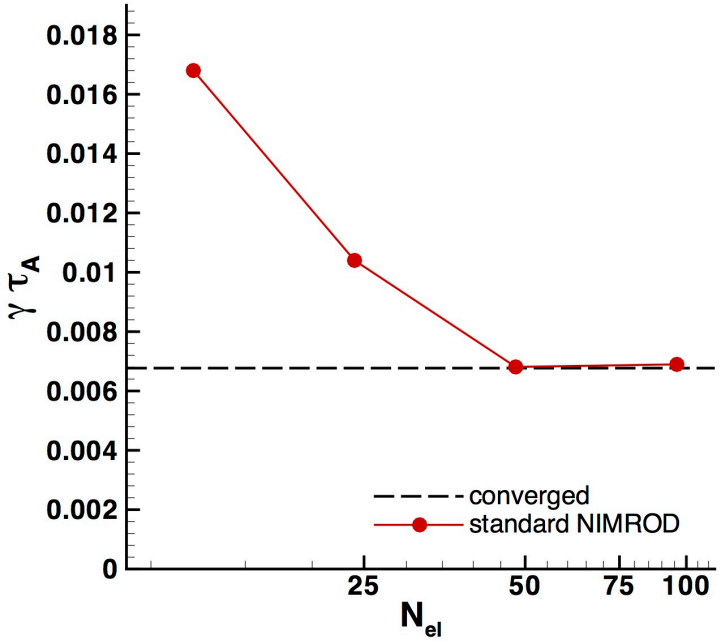

NIMROD results with its standard-methods converge from the unstable side.

- Reducing the polynomial degree for **V** in NIMROD admits numerical 0-frequency, mesh-scale modes that accumulate in nonlinear computations.

Spectral projection: Including numerical responses to the highest-order projections of flow divergence and of parallel vorticity helps stabilize the numerics.

- Spectral filtering has been used to stabilize spectral-element computations of incompressible flow. [Fischer and Mullen, *C. R. Acad. Sci. Paris* **332**, 265 (2001).]
  - In their paper, interpolation-based projection damps all vector-components of highest polynomial-degree for **V**.
  - It is used to stabilize computation at large Reynolds number.
- 'Spectral projection' for NIMROD means damping or propagating the highest-order Legendre polynomial in the spectral-element space.
- Projection can target specific behavior, such as divergence, perpendicular divergence, and/or parallel vorticity in MHD.

With NIMROD's 2D elements, divergence and parallel vorticity are projected onto Legendre polynomials that are of highest degree in one of the two logical coordinates.

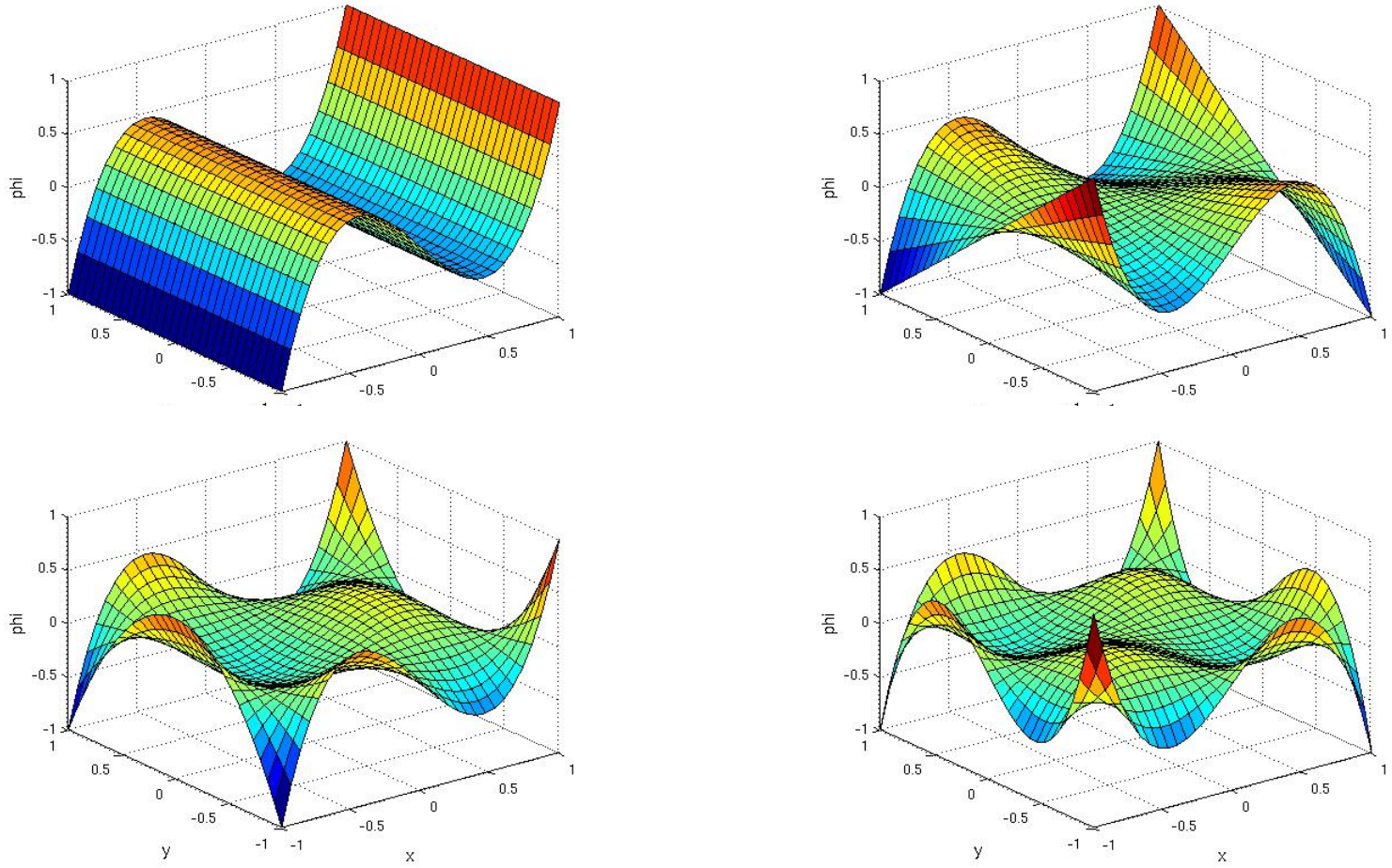

For bicubic V, the discontinuous fields for projection are *N*=3 Legendre polynomials in one of the two logical coordinates and a full expansion in the other. (4 of 7 shown)

Auxiliary fields associated with projection can be used for either hyperbolic or diffusive stabilization.

Hyperbolic (loosely):

$$\frac{d}{dt}\mathbf{V} = \rho^{-1}\mathbf{F} + f_d c_m \nabla\sigma + f_v c_A \hat{\mathbf{b}} \times \nabla\lambda$$

$$\frac{\partial}{\partial t}\sigma = f_d c_m \nabla \cdot \mathbf{V}$$

$$\frac{\partial}{\partial t}\lambda = f_v c_A \hat{\mathbf{b}} \cdot \nabla \times \mathbf{V}$$

Diffusive (loosely):

$$\frac{d}{dt}\mathbf{V} = \rho^{-1}\mathbf{F} + \left(d_d c_m^2 \Delta t\right)^{1/2} \nabla\sigma + \left(d_v c_A^2 \Delta t\right)^{1/2} \hat{\mathbf{b}} \times \nabla\lambda$$

$$\sigma = \left(d_d c_m^2 \Delta t\right)^{1/2} \nabla \cdot \mathbf{V}$$

$$\lambda = \left(d_v c_A^2 \Delta t\right)^{1/2} \hat{\mathbf{b}} \cdot \nabla \times \mathbf{V}$$

where **F** is the physical force density, c_A is the Alfven speed, c_m is the magneto-acoustic speed, and Δt is the NIMROD timestep.

The weak form of the hyperbolic approach shows how projection is implemented with spectral elements.

$$\int \rho \mathbf{W}^* \cdot \frac{d}{dt}\mathbf{V}\, dVol = \int \mathbf{W}^* \cdot \mathbf{F}\, dVol - f_d \int \sigma \left(\frac{B^2}{\mu_0} + \gamma P \right)^{1/2} \nabla \cdot \mathbf{W}^*\, dVol$$

$$- f_v \mu_0^{-1/2} \int \lambda \mathbf{B} \cdot \nabla \times \mathbf{W}^*\, dVol$$

$$\int \upsilon^* \frac{\partial}{\partial t}\sigma\, dVol = f_d \int \upsilon^* \left(\frac{B^2}{\mu_0} + \gamma P \right)^{1/2} \nabla \cdot \mathbf{V}\, dVol$$

$$\int \mu^* \frac{\partial}{\partial t}\lambda\, dVol = f_v \mu_0^{-1/2} \int \mu^* \mathbf{B} \cdot \nabla \times \mathbf{V}\, dVol$$

for all **W** in the continuous 3-vector space used for **V** and for all υ and μ in the discontinuous projection set used for σ and λ, respectively.

- Surface terms and gradients of background fields are discarded.
- Overlap with pressure and **J×B** responses only occurs at the limit of resolution, where the physics is represented poorly.

Projections in NIMROD: Linear and nonlinear tests substantiate the practicality and effectiveness of spectral projections.

- The implementation incorporates a new modal-basis module.
  - Routines for advancing **V** have new terms and equations for projecting divergence and parallel vorticity.
  - Coding for physical terms is unchanged.
- Tests of linear, initial-value behavior include:
  - The cylindrical profiles used with CYL_SPEC for testing local interchange,
  - Tearing modes (not discussed here), and
  - The circular cross-section, toroidal dens8 ELM profile from P. Snyder. [See Burke, *et al.*, PoP **17**, 032103 (2010).]
- Nonlinear tests include:
  - An unstable cylindrical interchange, and
  - The circular cross-section ELM problem.

Time-dependent, linear ideal-MHD NIMROD computations confirm the stabilizing effect when the divergence and vorticity projections include dissipation.

- Computations for a physically stable m=3, D_s=0.224 case show no growth over 10,000s of time-steps when a separate field is also used for magnetic divergence control.
- Convergence on the physically unstable m=4 is from the stable side.

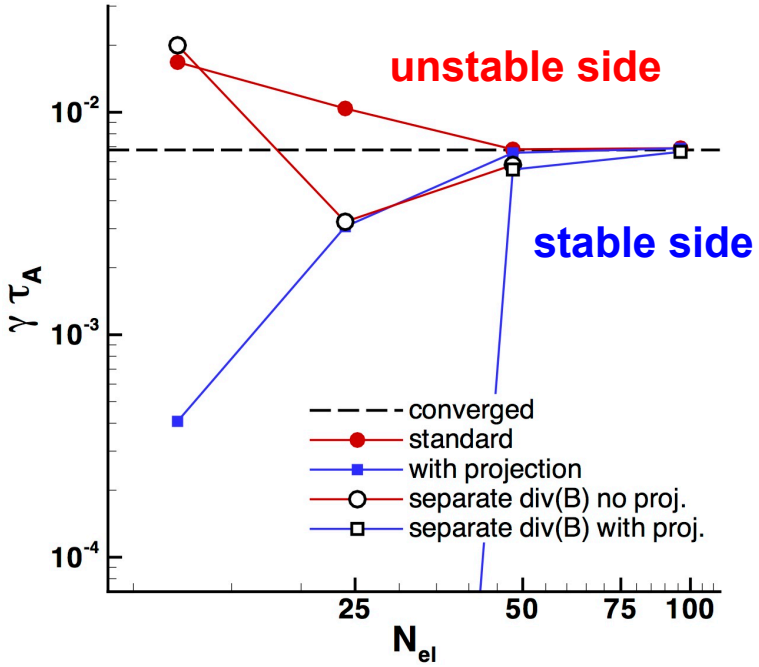

Comparison of NIMROD interchange convergence with different methods, all using biquartic elements.

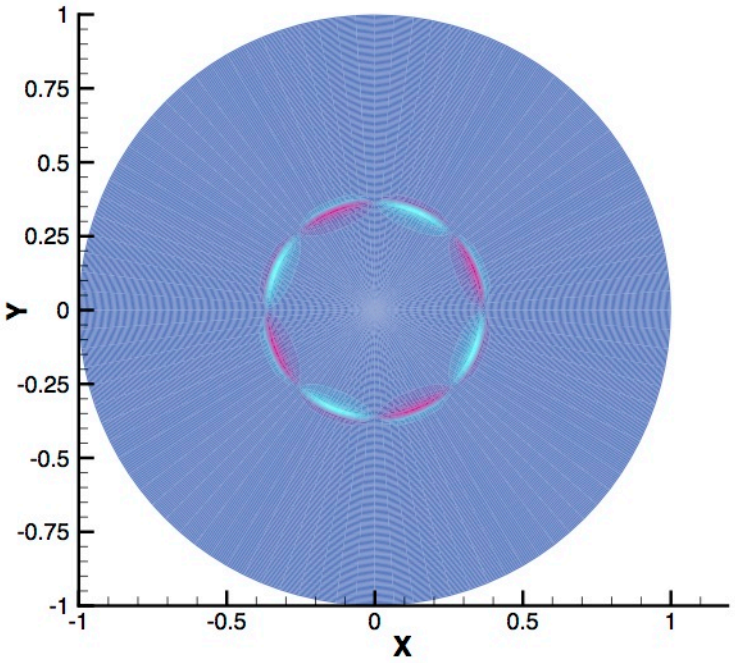

Contours of V_ϕ from the 48×24 case with projection and separate div(B) field.

A variant of the cylindrical problem that is physically unstable to interchange provides a nonlinear test.

- The region $0 \le r \le 0.466$ is Suydam-unstable.
- With $L_z=4\pi/3$, the (3,1) mode resonant at 0.265 and the (7,2) mode resonant at 0.404 are unstable. The (4,1) mode resonant at 0.5 is stable.
- $\tau_A = L_z/c_A = 4\pi/3$; $\tau_r = a^2\mu_0/\eta = 10^8$; Pm=10
- $D_n = \eta/\mu_0$; $\chi_{iso} = 10\eta/\mu_0$

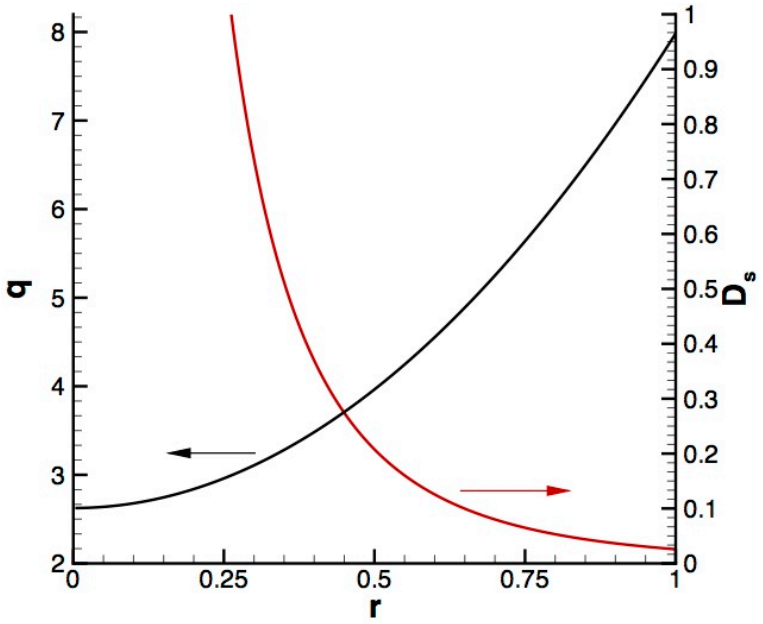

Safety factor and Suydam parameter for the nonlinear interchange computation.

- The computations use a 32x36 mesh of biquintic elements with 0≤n≤21 Fourier representation of the axial direction.
- The case with projection uses the diffusive method (d_d=1, d_v=0.3).

The computation with projection recovers from MHD events, whereas one without projection accumulates noise.

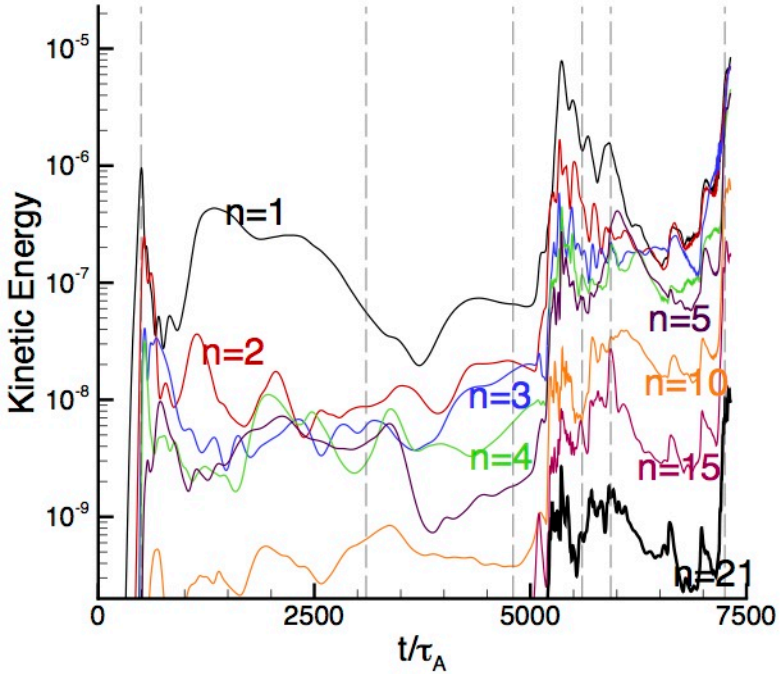

Kinetic fluctuation energies for the case with projection. (Vertical lines show times of contours on next slide.)

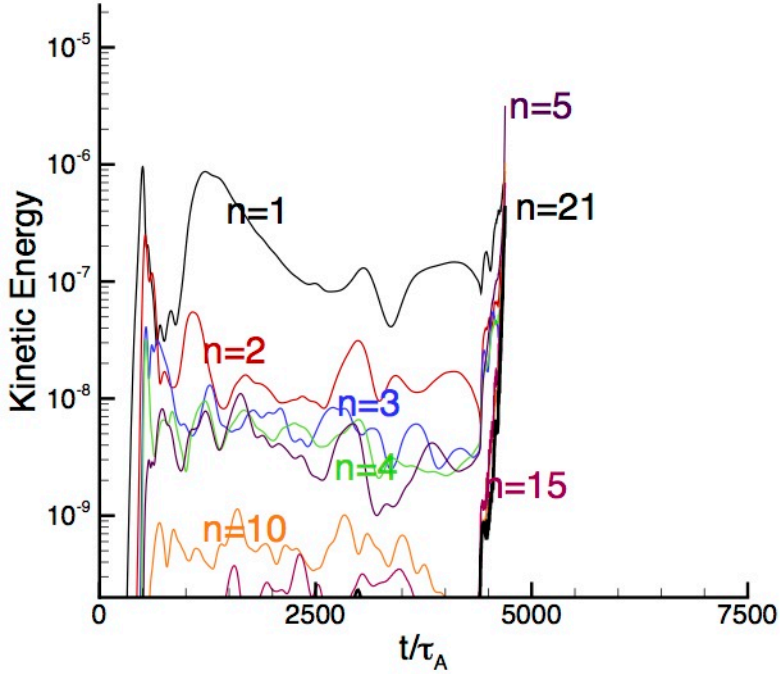

The spectrum computed without projection flattens, indicating accumulation of numerical noise.

- The computation with projection progresses into a turbulent stage.
- The computation without projection crashes as noise accumulates.

The evolution of pressure with projection shows a transition to turbulent transport.

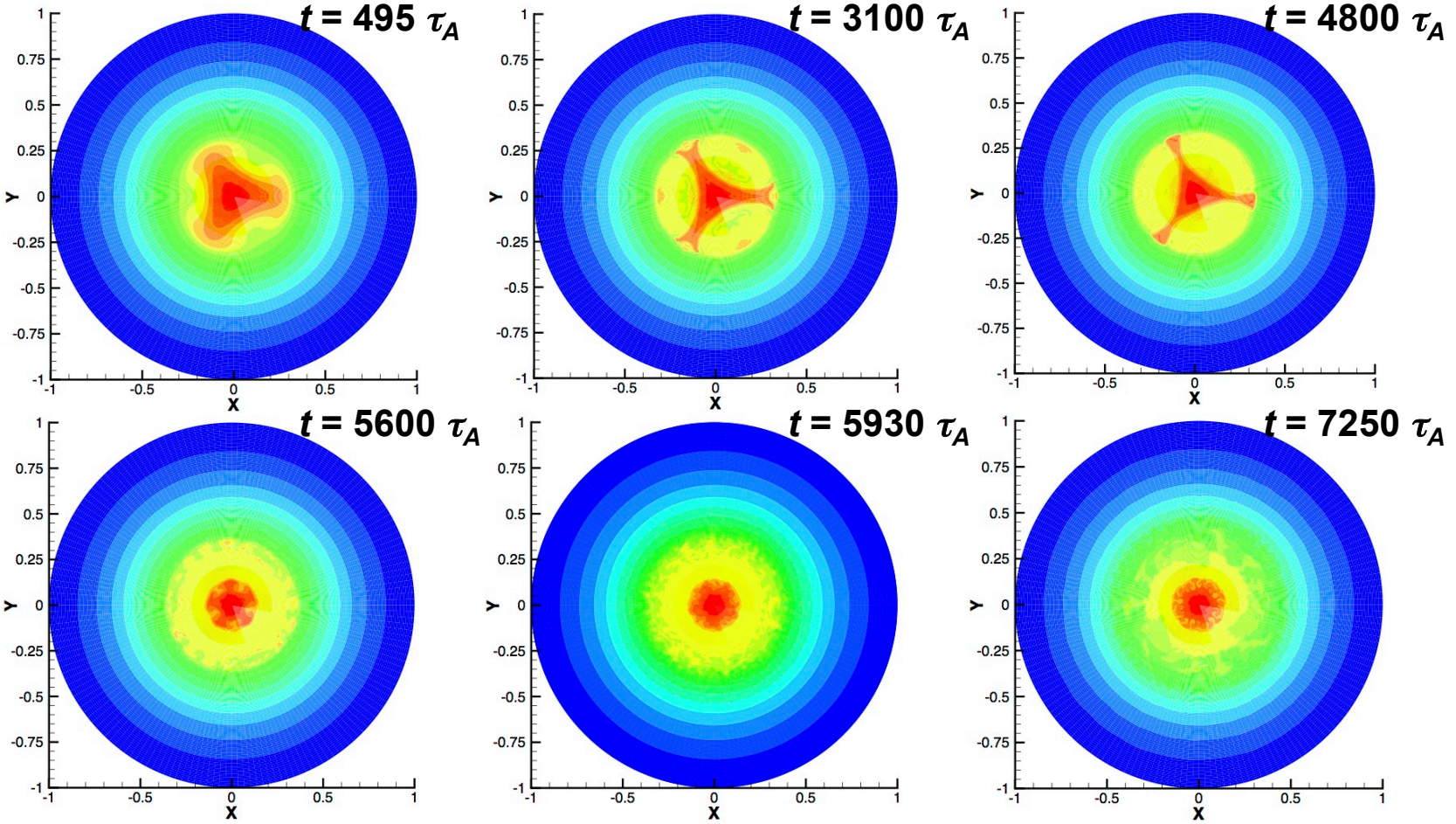

Sequence of pressure from the nonlinear interchange computation with projection shows an initial m=3 burst followed by multi-scale nonlinear fluctuation.

The successful evolution has fine-scale fluctuations without mesh-scale noise.

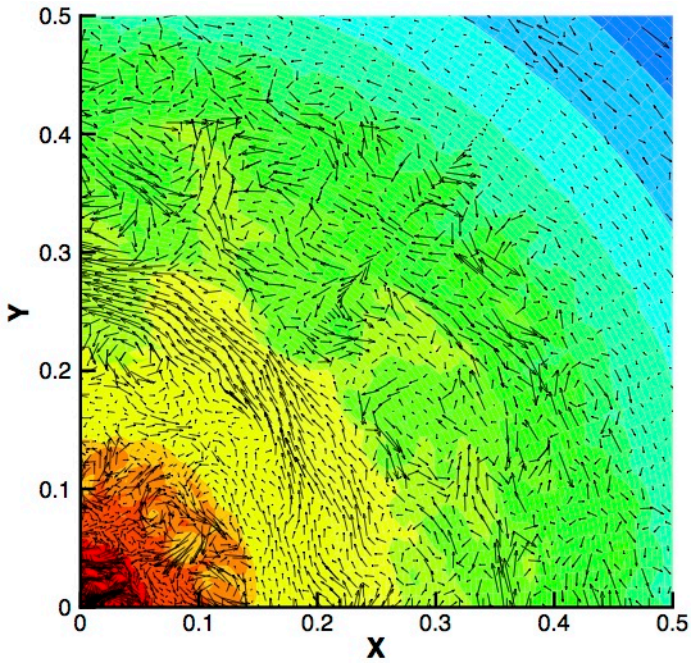

Velocity vectors overlaid on contours of pressure at the end of the computation with projection.

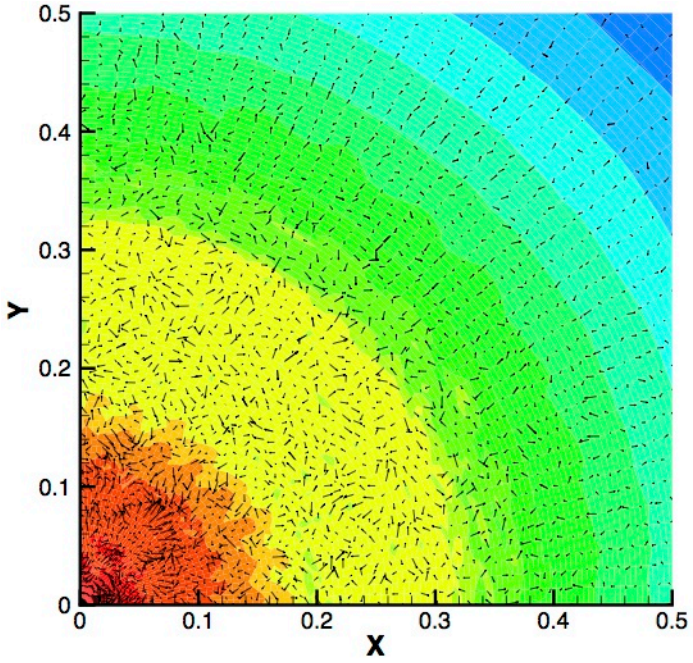

When the computation without projection leaves the laminar stage, its flow field becomes noisy.

- The computation with projection is not fully resolved, but robust progression facilitates nonlinear convergence.

Linear ELM computations also demonstrate convergence from the stable side with projection.

- We consider the standard, circular cross-section dens8 equilibrium as a starting point.
- All physical dissipation coefficients have the same small uniform value: $S=10^{10}$, Pm=1, etc.
- Like the interchange cases, projection leads to convergence from the stable side.

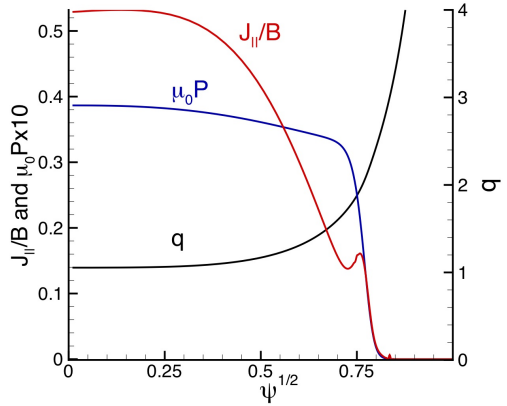

Equilibrium profiles for dens8.

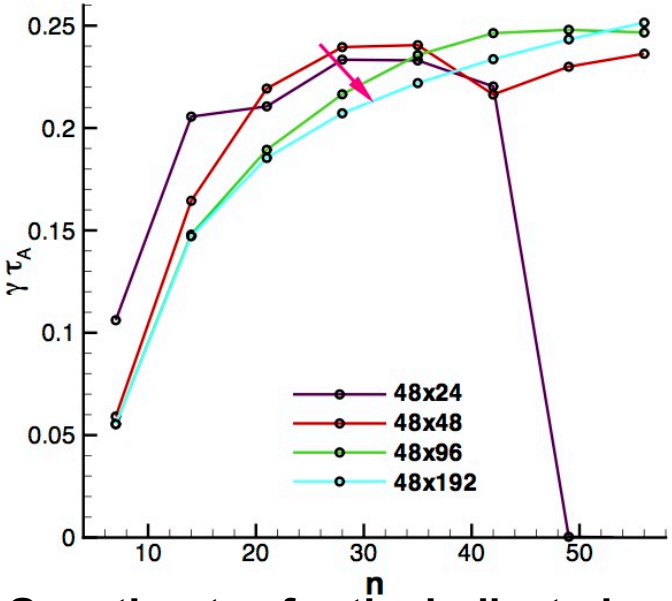

Growth rates for the indicated biquartic meshes without projection.

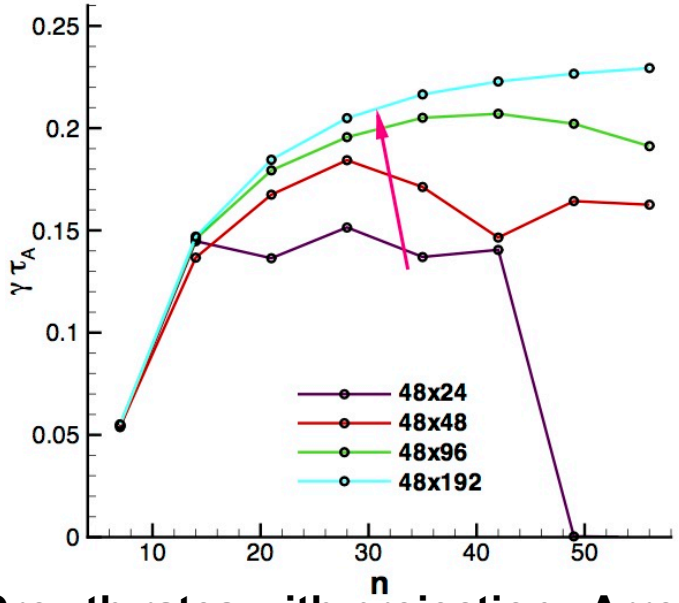

Growth rates with projection. Arrows show direction of convergence.

A nonlinear MHD computation from the same equilibrium exercises projection with a more violent instability.

- The domain imposes periodicity at 1/6th of the toroidal angle.
- Resistivity varies as $T^{-3/2}$ with S(0)=10^6; Pm=0.1; $\chi_{iso} = 0.01\eta/\mu_0$.
- Projective stabilization is also used in the continuity equation.

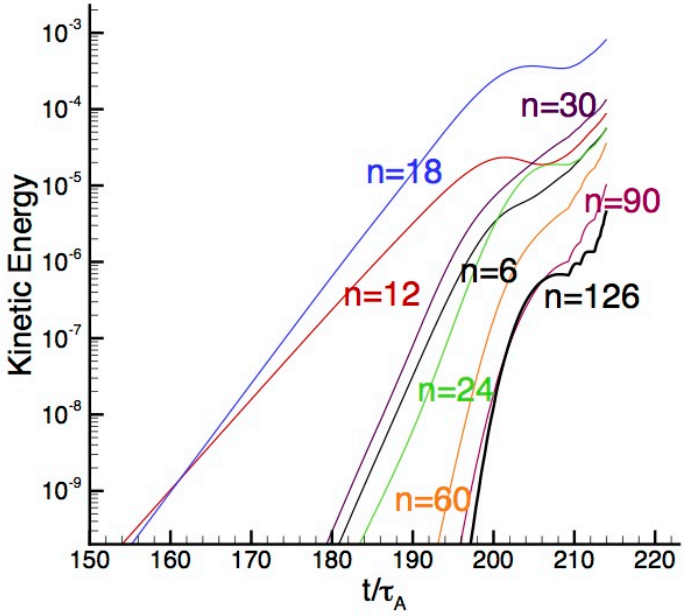

Selected kinetic fluctuation energies show that the largest-n remains small relative to others.

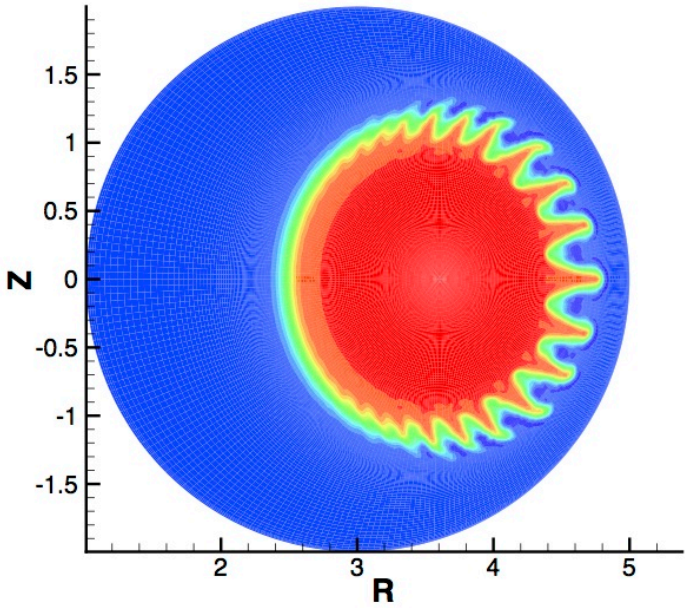

At t = 214 t_A in the computation, the ELM is expelling mass and energy from the pedestal; n is shown.

- Having stabilized flow, preserving monotonicity in the n and T evolution is now the most important consideration for fast dynamics.

Aside on DKE: The spectral-element form of the collision operator has been implemented and is more computationally efficient. [Held]

- A benchmark uses an NSTX equilibrium at realistic temperature.
- The DKE is the Hazeltine-equivalent form solved by NEO.

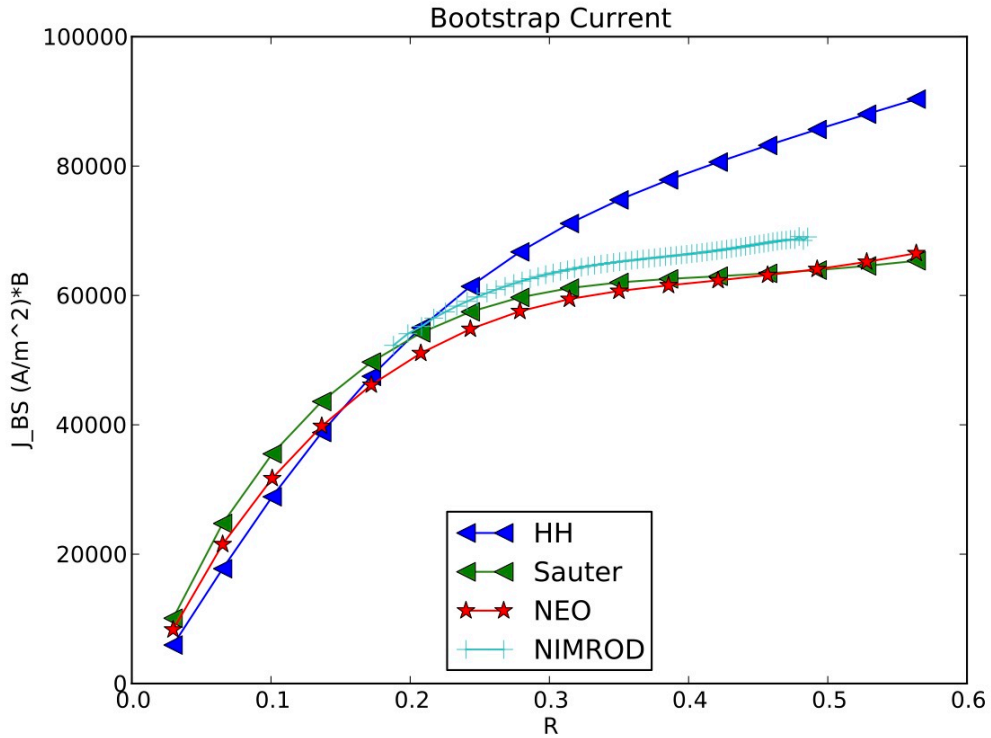

- The new implementation makes high-temperature computation practical.

Vacuum-field computations: Computing external magnetic field on a spectral-element mesh is an alternative to coupling Green's function solutions.

- Computational sub-domains can be assigned to solve the vacuum-distribution without advancing a plasma model.
- External solutions may be coupled by thin-wall approximation or by meshing a finite-thickness wall.
- Working directly with NIMROD's magnetic-field representation leads to a minimization problem at each time-step.
  - For the external subdomains, minimize

$$I_{vac} = \int_{R_{vac}} \left[\left(\nabla \times \mathbf{B} \right)^2 + \lambda_B \left(\nabla \cdot \mathbf{B} \right)^2 \right] dVol$$

subject to $\mathbf{B} \cdot \hat{\mathbf{n}}$ along ∂R_{vac}, consistent with coupling to the plasma-region.

The minimization computation has been implemented in NIMROD and tests match analytics.

- Tests are performed in a box that is periodic in one coordinate (ϕ).
- Solutions to boundary-value problems are products of sine waves and hyperbolic trigonometric functions.
- Two example results of vacuum-**B** from NIMROD are shown below.

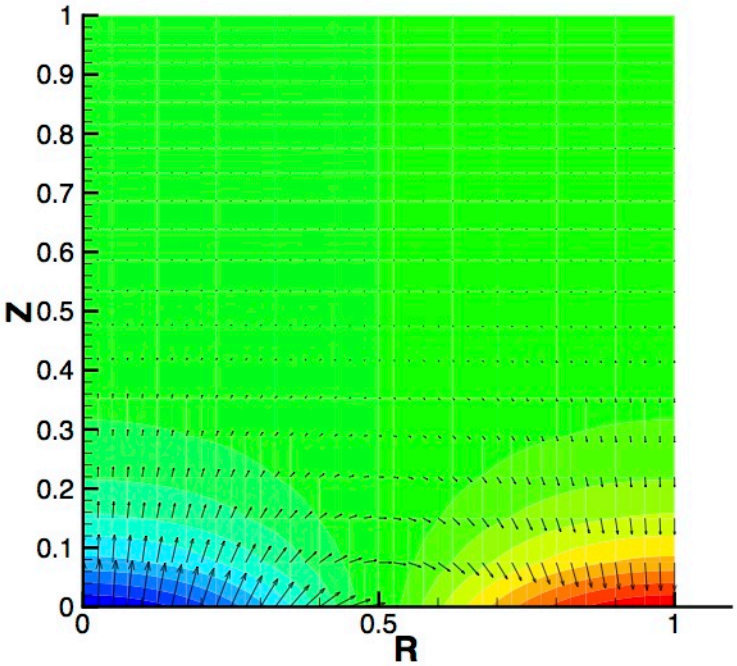

Boundary conditions impose half a wave on the bottom with n=1 variation in the perpendicular periodic coordinate.

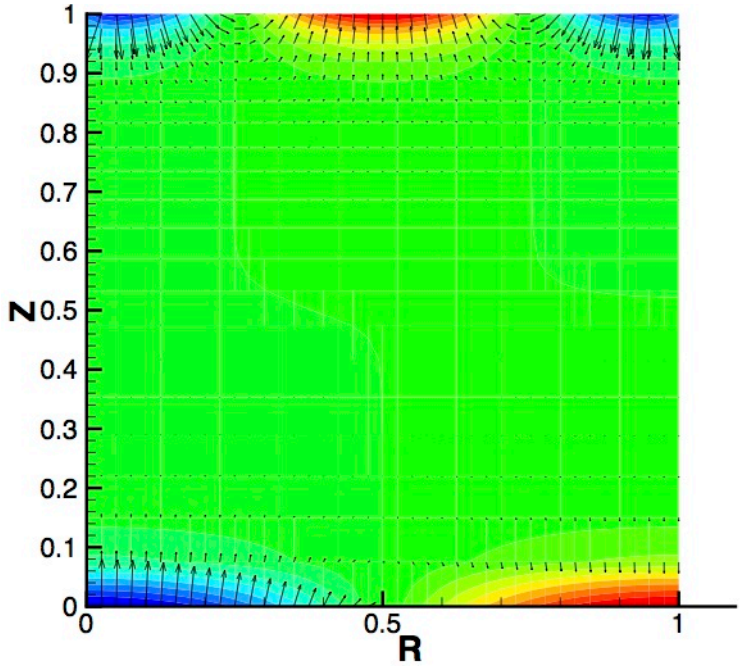

Here the bottom imposes half of a wave and the top imposes a full wave, both with n=3. [Implementation & tests by Kyle Bunkers.]

Conclusions

- Projecting parallel vorticity *and* flow-divergence at the limit of spectral-element resolution is a practical approach for controlling the convergence of numerical interchange. [See JP8.00125, Tues. PM for more analysis.]
  - Hyperbolic and diffusive methods are possible.
  - Tests in NIMROD confirm 1D CYL_SPEC eigenmode results.
- Diffusive projection provides smoothing of nonlinearly driven mesh-scale oscillations.
  - A nonlinear interchange problem successfully transitions to turbulent transport.
  - ELM computations progress into the late nonlinear phase.
- Computing vacuum-region magnetic field response with NIMROD's **B**-field representation is tractable.

NIMROD-Related Presentations at APS-DPP 2013

1. **Jenkins, BP8.00073** Active control of ECCD-induced tearing mode stabilization in coupled NIMROD/GENRAY HPC simulations
2. **Halfmoon, CP8.00058** Energetic Particle and Varying Aspect Ratio Effects on Resistive and Ideal MHD Modes
3. **McCollam, CP8.00068** MHD validation studies for RFPs
4. **Hebert, CP8.00117** NIMROD Modeling of Plasma Discharges in the Compact Toroidal Hybrid
5. **Necas, GP8.00037**, Rotational modes studies using NIMROD and HYM codes
6. **Hossack, GP8.00059** Measurements of Ion Temperature and Velocity in 80 -- 90 kA HIT-SI Discharges with Comparison to NIMROD Calculations
7. **Akcay, GP8.00060** Validation of the Resistive and Hall MHD Models of the HIT-SI with the NIMROD Code
8. **Morgan, GP8.00062** Two-fluid MHD simulation of the sustainment of closed flux by imposed dynamo current drive and the validation of mean dynamo theory
9. **Jarboe, GP8.00064**, A proof of principle spheromak experiment: The next step on a recently opened path to economical fusion power
10. **Howell, GP8.00069** Extended MHD Stabiliy Calculations of Spheromak Equilibria
11. **O'Bryan, JO4.00003** Simulation of current-filament dynamics and relaxation in the Pegasus ST
12. **Norgaard, JP8.00092**, Reacting Plasma-Neutral Fluid Simulations using the NIMROD Finite Element Code
13. **Nelson, JP8.00093** PSI-Center Simulations of Validation Platform Experiments
14. **Milroy, JP8.00094**, NIMROD validation using 3-axis probe data from the TCSU experiment
15. **Sauppe, JP8.00123** Helicity Conservation and Two-Fluid Relaxation Modeling for Reversed-Field Pinches
16. **Sovinec, JP8.00125** Verification of spectral stabilization and numerically modeled external vacuum in NIMROD
17. **Hooper, NP8.00023** Comparison of resistive MHD simulations and experimental CHI discharges in NSTX
18. **Ebrahimi, PI2.00002** Physics of fast flux closure in coaxial helicity injection experiments in NSTX
19. **Zhu, PP8.00060 NIMROD** Computation of Plasma Response to Resonant Magnetic Perturbations in DIII-D
20. **Montgomery, PP8.00066** Generalized resistive wall boundary conditions for cylindrical and toroidal geometry in NIMROD
21. **King, PP8.00072** Computational Investigation of Extended-MHD Effects on Tokamak Plasmas
22. **Mirnov, PP8.00115** Coexistence of drift-like and tearing instabilities in non-uniform plasma
23. **Woodruff, UP8.00016**, Extended MHD simulations for application to ITER disruption mitigation techniques
24. **Choi, YP8.00047**, Evaluation of Runaway Electrons with CQL3D/NIMROD and Validation with Measurements in DIII-D Tokamak